Observation-inferred resilience loss of the Amazon rain forest possibly due to internal climate variability

Raphael Grodofzig[1,2,4], Martin Renoult[2,3], and Thorsten Mauritsen[1,2]

[1]Department of Meteorology, Stockholm University, Stockholm, Sweden
[2]Bolin Centre for Climate Research, Stockholm University, Stockholm, Sweden
[3]Department of Geological Sciences, Stockholm University, Stockholm, Sweden
[4]Barcelona Supercomputing Center, Barcelona, Spain

Correspondence: Raphael Grodofzig (raphael.grodofzig@bsc.es)

Abstract. Recent observation-based studies suggest that the Amazon rain forest has lost substantial resilience since 1990, indicating that the forest might undergo a critical transition in the near future due to global warming and deforestation. The idea is to use trends in lag-1 auto-correlation of leaf density as an early warning signal of an imminent critical threshold for rain forest dieback. Here we test whether the observed change in auto-correlations could arise from internal variability by using historical and control simulations of nine sixth-generation Earth system model ensembles (Phase 6 of the Coupled Model Intercomparison Project, CMIP6). We quantify trends in leaf area index auto-correlation from both models and satellite observed vegetation optical depth from 1990 to 2017. Four models reproduce the observed trend with at least one historical realization, whereby the observations lie at the upper limit of model variability. Three out of these four models exhibit similar behavior in control runs, suggesting that historical forcing is not necessary for simulating the observed trends. Furthermore, we do not observe a critical transition in any future runs under the strongest greenhouse gas emission scenario (SSP5-8.5) until 2100 in the four models that best reproduce the past observed trends. Hence, the currently observed trends could be caused simply by internal variability, and, unless the data records are extended, have limited applicability as an early warning signal. Our results suggest that the current rapid decline in Amazon rain forest coverage is not foremost caused by global warming.

1 Introduction

The resilience level of the Amazon rain forest to external stresses, such as global warming and deforestation, is subject to ongoing debate (Feldpausch et al., 2016; Boers et al., 2017; Boulton et al., 2022). Since the 1970s the Amazon forest has lost about 20 percent of its coverage (Simmons et al., 2019) and the net carbon uptake of the formerly persistent carbon sink has been declining over the last four decades due to intensification of the dry season and elevated deforestation (Gatti et al., 2021). The rapid development has raised warnings that the Amazon forest is approaching a critical threshold, beyond which irreversible damage is unavoidable (Brando et al., 2014; Boers et al., 2017; Boulton et al., 2022; Parry et al., 2022; Doughty et al., 2023).

Model studies, however, differ widely in their results and the inter-model spread of vegetation responses in future projections remains high with moderate forest resilience this century, but a higher risk of sporadic rain forest loss past 2100 (Huntingford

et al., 2013; Boulton et al., 2017; Chai et al., 2021). Notably, Parry et al. (2022) found localized rain forest dieback using an abrupt-shift-detection algorithm in five out of seven CMIP6 models they investigated in simulations wherein CO_2 is increased by 1 percent per year until quadrupled after 140 years. All in all, though, climate models do not predict an imminent and complete collapse of the Amazon rain forest. However, it has been reported that climate models underestimate vegetation related feedbacks (Richardson et al., 2013; Green et al., 2017; Forkel et al., 2019).

Observation-based studies of the recent historical record convey a more alarming picture. Tao et al. (2022) reported the capacity of undamaged rain forests to withstand future droughts to be limited, especially in the Amazon. Analyzing remotely sensed vegetation data, Boulton et al. (2022) supported this idea and found that more than three quarters of the Amazon rain forest has been losing resilience since the 2000s, especially in regions of less rainfall and in proximity to regions of human activity. They present evidence for an imminent tipping point of the rain forest in the near future.

Such a tipping point may be initiated by a major tree loss from fires or deforestation, or climate change (Cox et al., 2008; Brando et al., 2014). Land cover transitions, such as forest-to-crop or forest-to-pasture, decrease the net surface radiation and latent heat flux, while increasing the sensible heat flux, resulting in warming of the land surface (Silvério et al., 2015). Reducing the vegetation density by deforestation is associated with enhanced precipitation run-off and reduced evapotranspiration. Hence, both deforestation and forest degradation by droughts weaken the moisture transport by recycling, which is mainly directed westwards over the Amazonian basin along the prevalent wind direction (Salati et al., 1979). This causes reduced precipitation downwind, and degraded forest health in a positive feedback loop.

Negative feedbacks and stabilising effects may also exist. For instance vegetation responds positively to increasing levels of CO_2 (Kolby Smith et al., 2016), provided sufficient water and nutrients are available, something which can be observed to happen in most parts of the world, including the Amazon basin (Zhu et al., 2016). Another possible mechanism could be convective clouds, that actively shift precipitation from wet to dry regions: the temperature gradient, arising from evaporative cooling in wet regions while warming dry regions, activates a low-level breeze that transports moisture to the dry areas (Hohenegger and Stevens, 2018). This, in extension would be a negative feedback in the Amazon in that the atmosphere acts to moisten dry regions. Since the Amazon rain forest has existed for at least thousands (Malhi et al., 2004), or even millions of years (Maslin et al., 2005), the rain forest must have been dominated by negative feedback in the past.

Tipping points are typically accompanied by a regime shift from a stable state where negative feedback mechanisms dominate, to a marginally stable state with transition to a net positive feedback parameter. Several statistical metrics, known as early warning signals, have been proposed to predict a regime shift (Scheffer et al., 2009; Lenton et al., 2012). Most commonly, they quantify the recovery rate of the system to small perturbations. The resilience of a system is subsequently defined as the ability to recover from those disturbances. As the stability of the system decreases, it recovers slower when stochastically forced. This phenomenon, known as critical slowing down (CSD), can be detected by an increase in lag-1 autocorrelation (AR(1)) of time series representing the dynamics of the system. Increasing AR(1) has been widely used as an early warning signal on Earth's dynamical systems such as the western Greenland ice sheet (Boers and Rypdal, 2021) or the Amazonian rain forest (Boulton et al., 2022). However, the increase in AR(1) has been shown to occur likewise for other physical reasons (Verbesselt et al.,

2016), as well as not occur prior to critical transitions, for instance when the rate of forcing is higher than the intrinsic response time scale for CSD (Boulton et al., 2013).

60   Here, we compare the observational record to nine large CMIP6 historical model ensembles and control simulations, quantifying model forest resilience between 1990 and 2014 using the same method as in Boulton et al. (2022). By analysing large model ensembles, we can test whether internal variability in auto-correlation could be the source of the observations-inferred resilience loss.

2   Methods

2.1   Data

65

We use the Amazon basin as our region of study, taken to be the domain defined as by RAISG - Amazon Network of Georeferenced Socio-Environmental Information, accessed March 2023. The observational data is provided by the Vegetation Optical Depth Climate Archive (VODCA) (Moesinger et al., 2020), which is available in a $0.25° \times 0.25°$ resolution in daily frequency for the period July 1987 to June 2017. The passive or active satellite observations capture the attenuation of microwave radi-
70   ation by vegetation, which is known as the vegetation optical depth (VOD). The attenuation depends on various factors like density, type and water content of the vegetation and the wavelength range of the sensor (Owe et al., 2008). Shorter wavelengths are more sensitive to upper leaf canopy than longer wavelengths, since they experience higher attenuation by vegetation. We chose the lowest wavelength product available (Ku-band, $\sim 19\,\mathrm{GHz}$) for the period January 1990 to December 2017, following the study by Boulton et al. (2022). The monthly means of the VODCA product are interpolated to $1° \times 1°$ for better comparing
75   to models, although this did not substantially affect the observed trend (see Fig. A1).

To assess internal variability, CMIP6 model ensembles with at least seven historical runs available and interactive leaf area index (LAI) are included in the study (Table 1). The non-dimensional LAI is defined as the total area of leaves per unit surface area. Although LAI and VOD are not identical variables, but physically closely related, changes in both variables are strongly correlated, such that they can be considered good proxies for forest health and resilience (Moesinger et al., 2020).

80   The model LAI output is evaluated in the period January 1990 to December 2014, as the historical experiments are only available until this point in time. Additionally, we use Shared Socioeconomic Pathway 5 (SSP5-8.5) and pre-industrial control simulations of 500 or 1000 years in length that we cut in windows of 25 years, corresponding to the length of the historical period. That way, we create a control ensemble of 20 or 40 members. Control simulations have the advantage that the internal variability of the model can be directly assessed since no external forcing is present.

85   The models' land surface components (Tab. 1) simulate exchanges of energy, water, and carbon between the land surface and the atmosphere, as well as biogeochemical processes like photosynthesis, of such LAI is computed dynamically in all models investigated. The ecosystem processes are mostly run on a daily time step, however CanESM5 and IPSL-CM6A run water and energy budget as well as photosynthesis computations on a sub-daily scale (in accordance with the atmospheric component). Only the two MPI-ESM1-2 models and EC-Earth3-Veg have simulated natural vegetation distribution, while all other models
90   investigated prescribe the plant functional type (PFT) fractions e.g. using the LUH2 v2h data set (Hurtt et al., 2020). How-

ever, the number of implemented PFTs differs widely from four (CanESM5) to 22 (CESM2). The nitrogen cycle is explicitly resolved in ACCESS-ESM1.5, CESM2, MIROC-ES2L, EC-EARTH-Veg3 and MPI-ESM1-2, while wildfires are deliberately modelled in CESM2 and the MPI-ESM1-2 family, occur randomly in EC-EARTH-Veg3 and are not considered in the other models (references see Tab. 1). Song et al. (2021) report generally good global representation of LAI in the GCMs in question.

In the Amazon, the multi-year (1982 – 2014) and yearly average is slightly underestimated by models, just as the inter-annual variability. Long-term LAI trends are generally captured but can vary in bias to observations in forested regions.

Lastly, we determine the land use and land cover change (LUCC) using the land use harmonization dataset LUH2 v2h and v2f (Hurtt et al., 2020), that is available as annual values on a $0.25° \times 0.25°$ spatial resolution and utilized to force the land components of CMIP6 models.

2.2 Resilience indicator AR(1)

The random variability of a signal contains information about the recovery rate from stochastic perturbations, such that we can separate trend, seasonality and residual of the signal using seasonal-trend decomposition (STL) by Loess (Cleveland et al., 1990). Assuming the seasonality is constant in time, we choose the STL input parameters trend = 19, season = 13 and period = 12 months, corresponding to choices made in previous work (Boulton et al., 2022). Nevertheless, slightly altering the STL parameters has no relevant influence on the presented results. The residual component of each grid cell can then be used to quantify the short-term responses of the forest by calculating the AR(1) on a sliding window of 5 years. We find the AR(1) time series by using an ordinary least-squares fitting method for the autoregressive model (Eq. 1), where ϵ_t represents white noise of the model with zero mean and constant variance σ_ϵ^2, X_t is the time series in each grid point and φ the autoregressive coefficient, also denoted AR(1).

$$X_t = \varphi X_{t-1} + \epsilon_t \tag{1}$$

We then quantify the trend of this AR(1) time series by Kendall's rank correlation τ_K that measures how well two data vectors agree on their ranks (Kendall, 1938). Choosing one vector to be time, a Kendall's $\tau_K = 1$ indicates a strictly increasing AR(1) trend, $\tau_K = -1$ a strictly decreasing and $\tau_K = 0$ no trend. The significance p of this statistic is computed by randomly generating phase surrogates of the time series' Fourier transform under constant variance and serial correlation (Dakos et al., 2008).

For comparison between observations and models, we calculate both the τ_K of the spatially averaged AR(1) series and for individual grid cells. The spatial distributions of τ_K are tested for similarity in frequency between observations and model using the non-parametric, two-sample Kolmogorov-Smirnov test (Berger and Zhou, 2014). Its test statistic is given by the maximum difference between two cumulative distribution functions and is computed under the null hypothesis that both samples are drawn from populations that have an arbitrary, yet identical, underlying distribution. The higher the p-value of this test, the less likely it is that the samples are drawn from different underlying distributions.

Table 1. CMIP6 model ensembles used within this study.

Model	Land surface model	Plant functional type	Nominal resolution	Number of hist. runs	Reference
ACCESS-ESM1-5	CABLE2.4	Prescribed	250 km	40	Ziehn et al. (2020)
IPSL-CM6A	ORCHIDEE v2	Prescribed	250 km	33	Boucher et al. (2020)
MPI-ESM1-2-LR	JSBACH 3.2	Simulated	250 km	30	Mauritsen et al. (2019)
MIROC-ES2L	MATSIRO6.0+VISIT-e v1	Prescribed	500 km	30	Hajima et al. (2020)
CanESM5	CLASS3.6-CTEM1.2	Prescribed	500 km	25	Swart et al. (2019)
MPI-ESM1-2-HR	JSBACH 3.2	Simulated	100 km	10	Mauritsen et al. (2019)
INM-CM5-0	INM-LND1	Prescribed	100 km	10	Volodin and Gritsun (2018)
CESM2	CLM5	Prescribed	100 km	9	Danabasoglu et al. (2020)
EC-EARTH3-Veg	HTESSEL	Simulated	100 km	7	Döscher et al. (2022)

3 Results

The observational record of auto-correlation of VOD from the Amazon basin exhibit variations and trends (Figure 1), but it is impossible based solely on a single data record to figure out whether such variations are caused by external forcing, or it is simply an expression of internal variability. A commonly used method to detect forced changes and events in observational records that contain internal and natural variability is to compare in various ways to multiple climate model runs with different codes and/or starting from different initial conditions (e.g. Hasselmann (1997), Otto (2023)). In particular it has become common that global climate models are run multiple times with the same historical boundary conditions, but starting from different initial conditions in order to explore their internal variability (Kay et al. (2015), Maher et al. (2021), Table 1). With such large ensembles it is possible to ask whether the observed trend is within the range of variability exhibited by the model, and in extension in the present case whether an increasing trend in auto-correlation constitutes a skillful early warning signal.

As an example, we display 30 simulations of the historical experiment of one CMIP6 model, MPI-ESM1-2-LR, together with the observations (Figure 1, right panel). We see that the observed trend in spatially averaged AR(1) of $\tau_K = 0.62$ is within the range of trends exhibited by the model ensemble members (-0.76 to 0.72) when calculated over the same period. Therefore, in terms of this model's behavior the observed trend is within the range of variability. To investigate whether global warming or land-use change is affecting the trends we can also inspect equally long duration chunks from the same model's pre-industrial control simulation (Figure 1, left panel). Here we also find trends that encapsulate the observed trend (-0.68 to 0.79). Even though the shorter term deviations appear slightly muted in this case compared to the historical ensemble, the overall trend range in control and historical experiment does only differ marginally. Moreover, the largest AR(1) trend of this model is found among the control runs, suggesting that the forced response of the Amazon rain forest is not needed to generate an increase in AR(1) of similar magnitude to that observed.
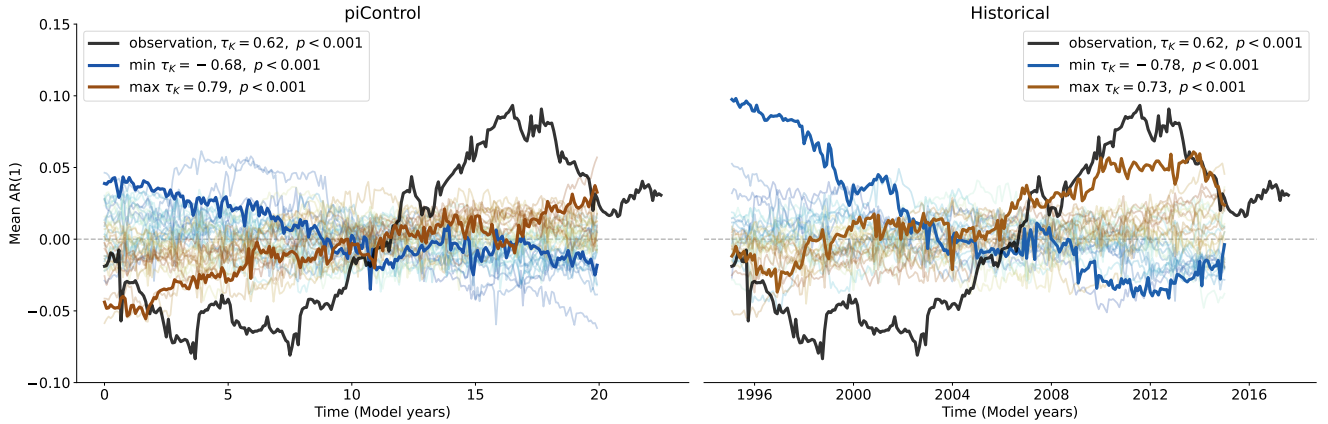
Figure 1. Anomaly of the spatially averaged AR(1) series for observations and MPI-ESM1-2-LR piControl (left panel) and historical (right panel) ensemble. The anomaly is computed by subtracting the temporal mean from the time series, and is plotted at the end of the 5 years sliding window. The ensemble member with the largest and smallest τ_K are highlighted. The color gradient of all ensemble runs corresponds to increasing τ_K.

The modelled spatial distributions of the trends in AR(1) further support the idea that the origin is internal variability. We can inspect maps and frequency distributions from the two historical ensemble members and the two chunks from the pre-industrial control in Figure 2 that exhibited the largest trends (Figure 1). All historical ensemble members are shown in Figure A2. We see that positive trends can occur in any part of the Amazon basin, and are not preferentially occurring in the southern parts where most of the land use changes happened (Figure A6). There are, however, cases wherein this pattern occurs (e.g. members 4, 13, 15, 26 and 30). Also noteworthy is that the model does display trend patterns with spatial scales that are substantially larger than the model resolution such that the underlying causes must be a simulated feature of the model, e.g. large scale weather events.

Not all models are equally fit for the purpose of simulating the Amazon rain forest dynamics in accordance with observations. To investigate this, we apply the Kolmogorov-Smirnov (KS) test (Section 2.2) on each ensemble member to test whether it could have been drawn from the same underlying distribution as the observations. The process is illustrated in Figure 3. For the MPI-ESM1-2-LR model the test identifies two ensemble members (5 and 28) that are statistically indistinguishable from the observed trend distribution. This implies that the observations lie within the range of model variability, but on the edge of what the model is able to reproduce. We carry out the same procedure for all models and find that four of the nine models pass the test (Table 2) with CanESM5 (Fig. A3), ACCESS-ESM1-5 (Fig. A4) and MIROC-ES2L (Fig. A5) showing closer affinity to observations than the MPI-ESM1-2-LR model which we have focused on thus far.

A drawback of applying the KS test method here is that some model ensembles may be too small, and therefore simply by chance none of the ensemble members pass the KS test, even if the model is capable of producing such a simulation. Indeed, we see that four of the five models that are not passing the KS test have 10 or fewer historical ensemble members. For example
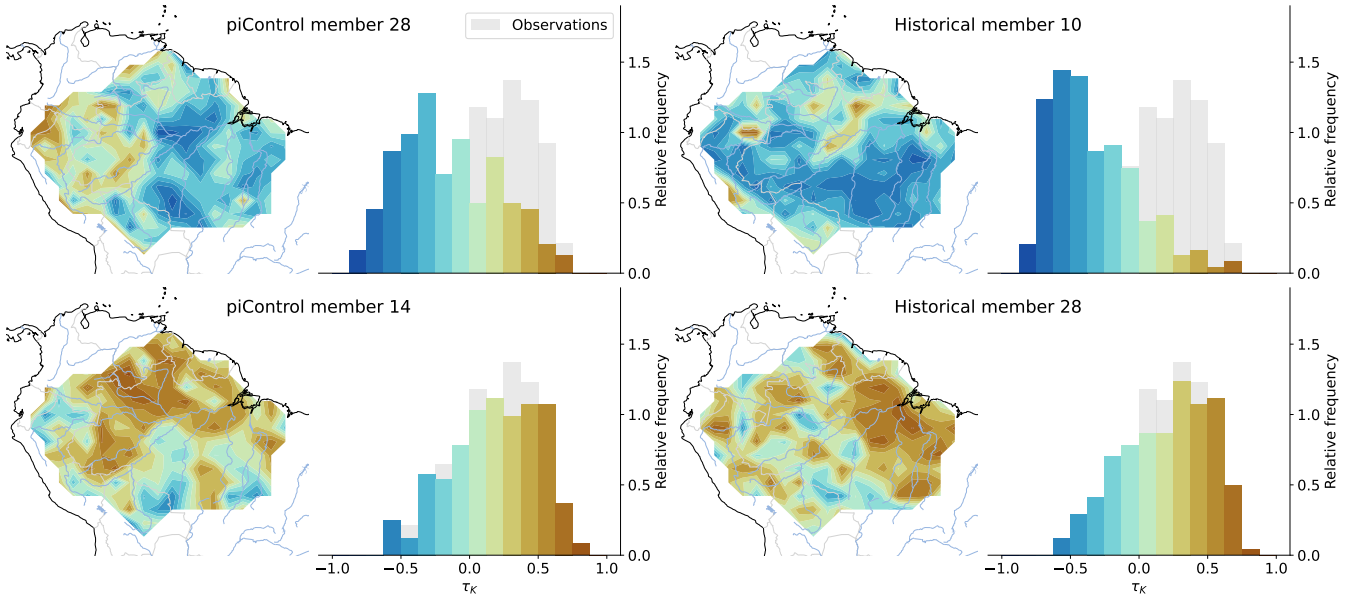
Figure 2. Maps and histograms of the τ_K values of selected members from the piControl (left panels) and historical (right panels) MPI-ESM1-2-LR ensemble. The observed τ_K distribution is plotted in grey for comparison. We selected the ensemble members that have the highest and lowest τ_K of the spatially averaged AR(1) series to present the full range of model variability.

MPI-ESM1-2-HR is physically very similar to MPI-ESM1-2-LR, with the main difference of applying a higher resolution resulting in fewer simulated members: 10 instead of 30. Therefore it is plausible that also this model is fit for purpose, but it was not run enough times to demonstrate that. The only exception to this rule is IPSL-CM6A, which with 33 ensemble members is more unlikely to have a plausible representation of Amazon vegetation dynamics.

Inspecting the Amazon mean trend of AR(1) for each of the ensemble members from the four models that passed the KS test we find one model which displays a significant response to historical forcing (MIROC-ES2L, Figure 4). To better show the shift between the pre-industrial control and historical simulations we fit a bounded beta-distribution to the frequency distribution, of which we use the $\alpha = 0.95$ confidence interval to screen for significance. In all four models and for both simulations the observed trend is on the edge of what is possible. In CanESM5, MPI-ESM1-2-LR and ACCESS-ESM1-5 there is not a substantial difference between the forced and unforced simulations, but MIROC-ES2L shows a marked shift towards higher trends in Amazon basin mean AR(1) when the model is exposed to historical boundary conditions.

We finally test the idea that an increasing AR(1) can be used as an early-warning signal of an eminent abrupt transition in the Amazon rain forest. This was done by inspecting the continuation future projections of the two historical runs with largest positive and negative historical trends from MPI-ESM1-2-LR (Fig. 5). This is the Shared Socioeconomic Pathway 5 with a radiative forcing of about $8.5\,\mathrm{W/m^2}$ at the end of the Century (SSP5-8.5). Under this strong forcing future scenario the model exhibits a slight increasing trend in AR(1), along with a decreasing trend of LAI of on average $-0.05\,\mathrm{m^2 m^{-2}}$. Neither of the
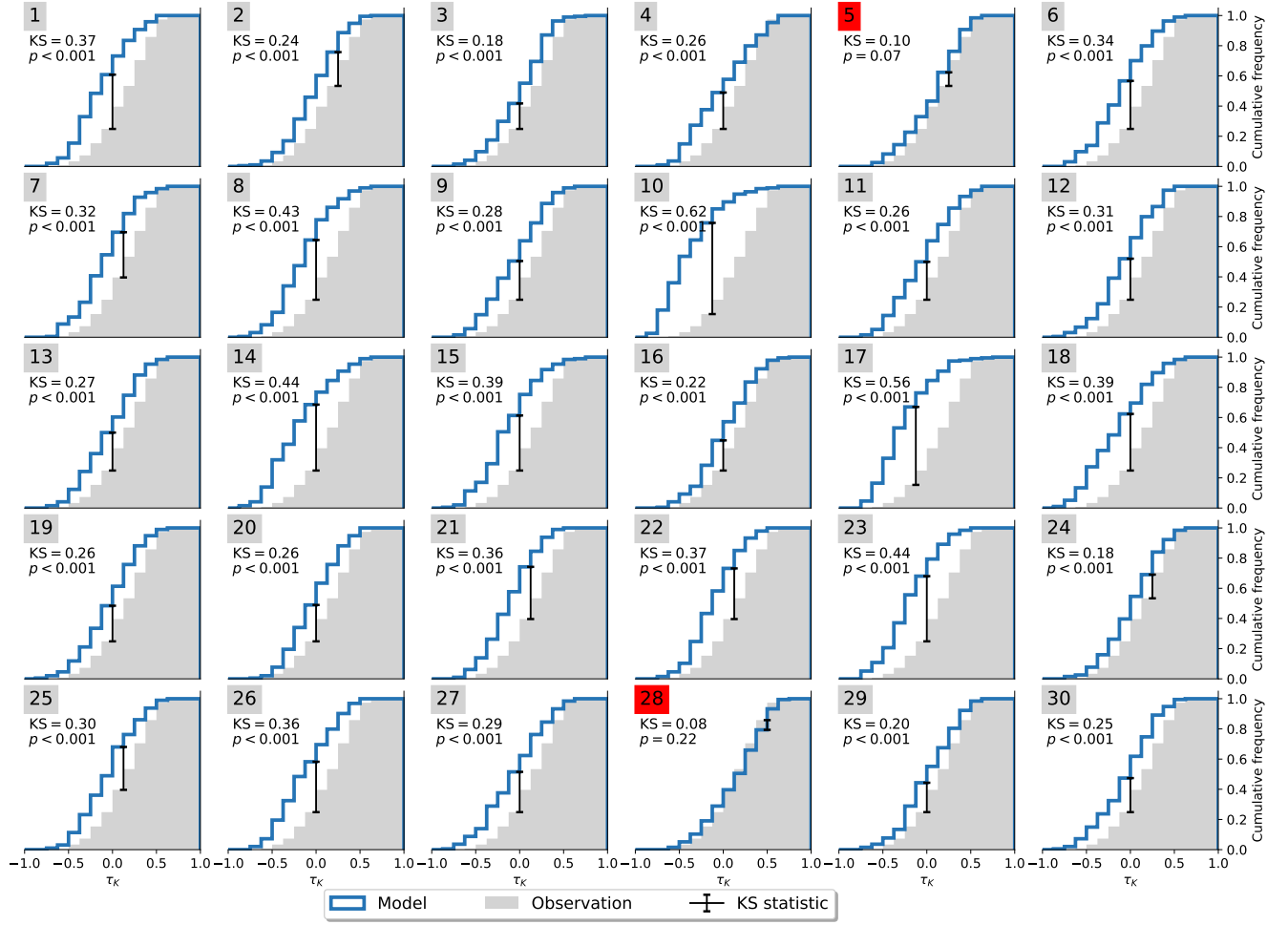
Figure 3. Cumulative distribution functions of τ_K for observations and members of MPI-ESM1-2-LR. The KS-statistic is drawn as a black error bar. Members that are not significantly different from the observational distribution are marked in red. Member 28 shows best agreement with KS = 0.08 and $p = 0.22$.

two extreme runs, nor any other ensemble members exhibit an abrupt decline in LAI. In fact, we do not observe a regime shift in any of the other four models that passed the KS test. The linear deterioration of forest viability can be caused by a variety of factors including limited water availability or progressing land use change (Fig. A7). However, the changes induced by future forcing do not facilitate bifurcation-like behavior of the system.

Table 2. Observation's percentiles p_{cml} in mean τ_K model distribution, fraction of ensemble members $F_{p>0.05}$ that scored $p > 0.05$ in the KS-test and highest KS-test p-value of each ensemble. The higher the p-value, the more likely the member resembles the observations. p_{cml} represents the fraction of mean τ_K values of a model that are higher than the observational mean τ_K (see Fig. 4). Displayed for all nine historical ensembles and the control ensembles of the four well-agreeing historical ensembles. piControl ensembles are run under pre-industrial conditions. Well-agreeing ensembles have at least one member that does not significantly differ from the observations according to the KS test.

Model	historical			piControl		
	p_{cml} of $\overline{\tau}_K$	KS-test $F_{p>0.05}$	KS-test highest p (member)	p_{cml} of $\overline{\tau}_K$	KS-test $F_{p>0.05}$	KS-test highest p (member)
MIROC-ES2L	0.04	6/30	0.97 (13)	< 0.01	1/20	0.29 (9)
ACCESS-ESM1-5	0.02	3/40	0.56 (13)	0.01	1/20	0.21 (12)
CanESM5	< 0.01	2/25	0.75 (24)	0.02	4/40	0.84 (20)
MPI-ESM1-2-LR	0.01	2/30	0.22 (28)	0.02	3/40	0.40 (14)
MPI-ESM1-2-HR	< 0.01	0/10	< 0.05 (-)			
CESM2	< 0.01	0/9	< 0.05 (-)			
EC-EARTH3-Veg	< 0.01	0/7	< 0.05 (-)			
IPSL-CM6A	< 0.01	0/33	< 0.05 (-)			
INM-CM5-0	< 0.01	0/10	< 0.05 (-)			

4 Conclusions

In this study we have tested the idea that trends in the persistence of vegetation density anomalies can be used as an early warning signal for Amazonian rain forest. This is particularly concerning upon the backdrop of a large observed trend since 1991, suggesting that the forest has undergone a pronounced loss of resilience (Boulton et al., 2022). The trend in anomaly persistence is quantified through the lag-1 year correlation, AR(1).

To this end, we inspect simulations from nine Earth system model ensembles initialized with different initial conditions in 1850, such that variations within each ensemble are an expression of internal variability simulated by that particular model. We find that four of the models have ensemble members that are statistically indistinguishable from the observed trend. Four other models with 10 or fewer realisations did not have a matching realisation, and one model with 33 realisations did clearly underperform. Of the four well performing model ensembles, three of them showed trends similar to observations also in their unforced control simulations. These results suggest that the observed trend could simply be an expression of internal variability, and that longer data records would be needed to show that the opposite is the case.

This result is further corroborated by the spatial distribution of the increasing trend in AR(1) in the model simulations. Here it is found that ensemble members with substantial positive or negative trends show these in relatively large regions, but not necessarily in those regions with large anthropogenic deforestation. This suggests that such anomalies could be associated with large scale weather events.
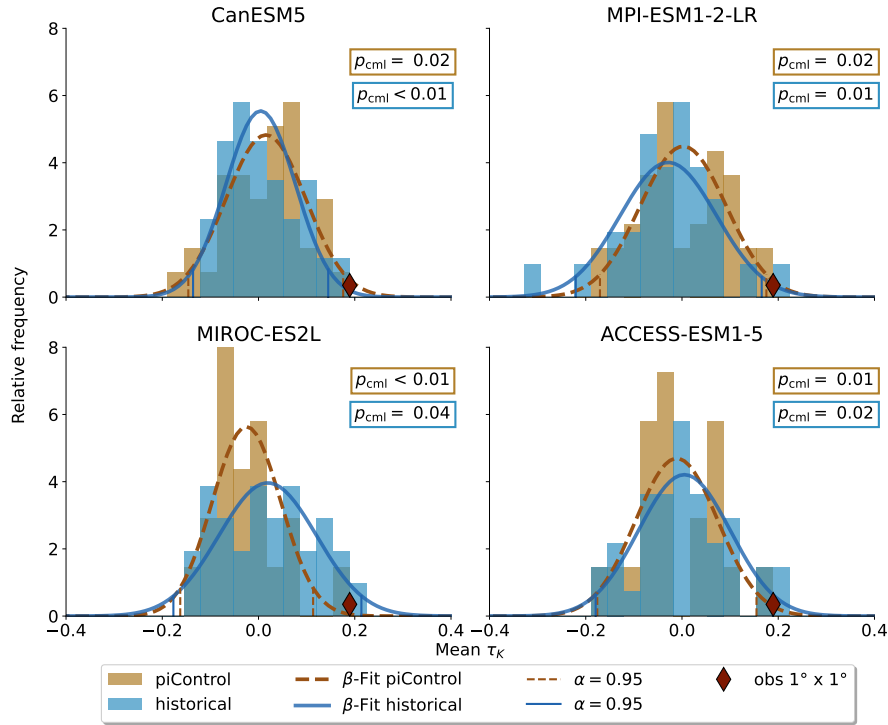
Figure 4. Model's mean τ_K distributions for piControl and historical runs. The histograms are fitted with a β-distribution on the interval $[-1, 1]$. The observation's percentile within the respective distribution is denoted by p_{cml}. Historical forcing makes the occurrence of the observations more likely only in MIROC-ES2L and ACCESS-ESM1-5, while CanESM5 and MPI-ESM1-2 simulate a higher probability in control runs.

We finally check whether trends in AR(1) can be used as an early warning signal by investigating the relationship between the recent past and the rain forest evolution in future strong warming scenario projections (SSP5-8.5). However, there is no such relationship, and furthermore none of the future simulations exhibit rapid transitions.

It is worth noting that even if the results presented here suggest that the Amazon rain forest has not lost its resilience, and is unlikely to undergo bifurcations in the future, it does not mean the forest is invulnerable to human caused stresses from global warming, deforestation and fires. On the contrary, the results presented here suggest that global warming as a major historical and future forcing in models plays a minor role in the observed rapid decline in rain forest extent. Mitigation strategies to limit future rain forest loss could therefore be most effective focusing on other human-induced stress factors.

Data availability. The data of the CMIP6 models can be downloaded from ESGF Portal at DKRZ, located at https://esgf-data.dkrz.de/projects/esgf-dkrz/ (last access: 15 May 2023). The observational VOD data is available on https://doi.org/10.5281/zenodo.2575599 (last access: 18 March
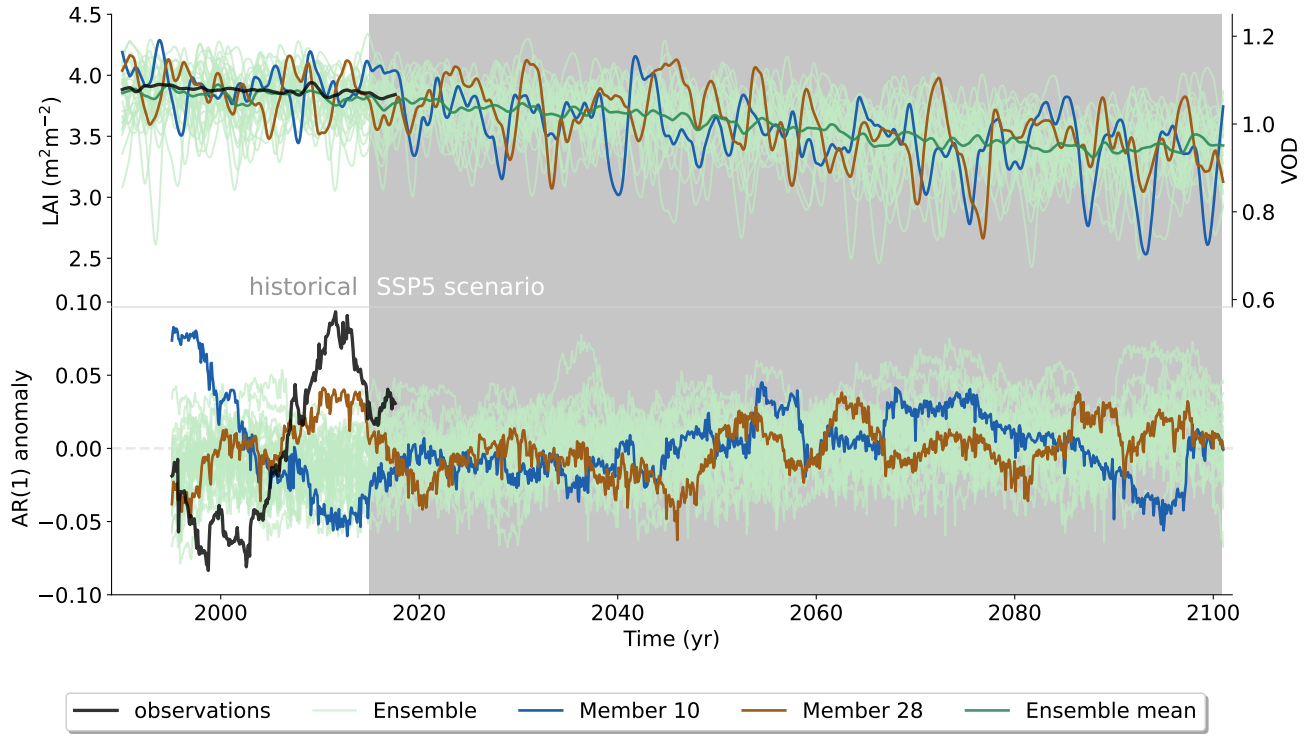
Figure 5. Historical and SSP5-8.5 scenario of MPI-ESM1-2-LR LAI and corresponding spatially averaged AR(1) trend compared to the observational VOD record. Upper panel displays the STL trend component of LAI and VOD respectively, lower panel shows the AR(1) series of the STL residual plotted at the end of the 5 years sliding window. Ensemble member 28 is the best-agreeing member with observations in the historical period, member 10 the least agreeing. Note that the dual vertical axes used in the upper panel are scaled to have the same relative range.

2023). Land use and land cover data can be found on https://luh.umd.edu/index.shtml (last access: 21 April 2023). The outlines of the Amazon forest are taken from RAISG https://www.raisg.org/en/ (last access: 10 March 2023).

210 *Author contributions.* RG carried out the analysis and drafted the paper with inputs from MR and TM. All authors contributed to the study.

Competing interests. The contact author has declared that none of the authors has any competing interests.

Acknowledgements. This work was supported through funding from the Swedish Research Council (VR), Grant agreement 2022-03262, the European Research Council (ERC) Grant agreement 770765 and the European Union's Horizon 2020 program Grant agreements 820829 and 101003470. We acknowledge the World Climate Research Program, which is in charge of CMIP, and thank the climate modeling groups (listed in Table 1 in the Methods section) for producing and publishing their model output. We acknowledge equally Moesinger et al. (2020) for creating the global long-term VOD Climate Archive (VODCA) and making their data available.

References

Berger, V. W. and Zhou, Y.: Kolmogorov–Smirnov Test: Overview, in: Wiley StatsRef: Statistics Reference Online, John Wiley & Sons, Ltd, https://onlinelibrary.wiley.com/doi/abs/10.1002/9781118445112.stat06558, 2014.

220 Boers, N. and Rypdal, M.: Critical slowing down suggests that the western Greenland Ice Sheet is close to a tipping point, Proceedings of the National Academy of Sciences, 118, e2024192 118, https://doi.org/10.1073/pnas.2024192118, 2021.

Boers, N., Marwan, N., Barbosa, H. M. J., and Kurths, J.: A deforestation-induced tipping point for the South American monsoon system, Scientific Reports, 7, 41 489, https://doi.org/10.1038/srep41489, 2017.

Boucher, O., Servonnat, J., Albright, A. L., Aumont, O., Balkanski, Y., Bastrikov, V., Bekki, S., Bonnet, R., Bony, S., Bopp, L., Braconnot,
225 P., Brockmann, P., Cadule, P., Caubel, A., Cheruy, F., Codron, F., Cozic, A., Cugnet, D., D'Andrea, F., Davini, P., de Lavergne, C., Denvil, S., Deshayes, J., Devilliers, M., Ducharne, A., Dufresne, J.-L., Dupont, E., Éthé, C., Fairhead, L., Falletti, L., Flavoni, S., Foujols, M.-A., Gardoll, S., Gastineau, G., Ghattas, J., Grandpeix, J.-Y., Guenet, B., Guez, Lionel, E., Guilyardi, E., Guimberteau, M., Hauglustaine, D., Hourdin, F., Idelkadi, A., Joussaume, S., Kageyama, M., Khodri, M., Krinner, G., Lebas, N., Levavasseur, G., Lévy, C., Li, L., Lott, F., Lurton, T., Luyssaert, S., Madec, G., Madeleine, J.-B., Maignan, F., Marchand, M., Marti, O., Mellul, L., Meurdesoif, Y., Mignot, J., Musat,
230 I., Ottlé, C., Peylin, P., Planton, Y., Polcher, J., Rio, C., Rochetin, N., Rousset, C., Sepulchre, P., Sima, A., Swingedouw, D., Thiéblemont, R., Traore, A. K., Vancoppenolle, M., Vial, J., Vialard, J., Viovy, N., and Vuichard, N.: Presentation and Evaluation of the IPSL-CM6A-LR Climate Model, Journal of Advances in Modeling Earth Systems, 12, e2019MS002 010, https://doi.org/10.1029/2019MS002010, 2020.

Boulton, C. A., Good, P., and Lenton, T. M.: Early warning signals of simulated Amazon rainforest dieback, Theoretical Ecology, 6, 373–384, https://doi.org/10.1007/s12080-013-0191-7, 2013.

235 Boulton, C. A., Booth, B. B. B., and Good, P.: Exploring uncertainty of Amazon dieback in a perturbed parameter Earth system ensemble, Global Change Biology, 23, 5032–5044, https://doi.org/10.1111/gcb.13733, 2017.

Boulton, C. A., Lenton, T. M., and Boers, N.: Pronounced loss of Amazon rainforest resilience since the early 2000s, Nature Climate Change, 12, 271–278, https://doi.org/10.1038/s41558-022-01287-8, 2022.

Brando, P. M., Balch, J. K., Nepstad, D. C., Morton, D. C., Putz, F. E., Coe, M. T., Silvério, D., Macedo, M. N., Davidson, E. A., Nóbrega,
240 C. C., Alencar, A., and Soares-Filho, B. S.: Abrupt increases in Amazonian tree mortality due to drought–fire interactions, Proceedings of the National Academy of Sciences, 111, 6347–6352, https://doi.org/10.1073/pnas.1305499111, 2014.

Chai, Y., Martins, G., Nobre, C., von Randow, C., Chen, T., and Dolman, H.: Constraining Amazonian land surface temperature sensitivity to precipitation and the probability of forest dieback, npj Climate and Atmospheric Science, 4, 1–7, https://doi.org/10.1038/s41612-021-00162-1, 2021.

245 Cleveland, Cleveland, William S, McRae, Jean E, and Terpenning, Irma: STL: A seasonal-trend decomposition, J. Off. Stat, 6, 3–73, 1990.

Cox, P. M., Harris, P. P., Huntingford, C., Betts, R. A., Collins, M., Jones, C. D., Jupp, T. E., Marengo, J. A., and Nobre, C. A.: Increasing risk of Amazonian drought due to decreasing aerosol pollution, Nature, 453, 212–215, https://doi.org/10.1038/nature06960, 2008.

Dakos, V., Scheffer, M., van Nes, E. H., Brovkin, V., Petoukhov, V., and Held, H.: Slowing down as an early warning signal for abrupt climate change, Proceedings of the National Academy of Sciences, 105, 14 308–14 312, https://doi.org/10.1073/pnas.0802430105, 2008.

250 Danabasoglu, G., Lamarque, J.-F., Bacmeister, J., Bailey, D. A., DuVivier, A. K., Edwards, J., Emmons, L. K., Fasullo, J., Garcia, R., Gettelman, A., Hannay, C., Holland, M. M., Large, W. G., Lauritzen, P. H., Lawrence, D. M., Lenaerts, J. T. M., Lindsay, K., Lipscomb, W. H., Mills, M. J., Neale, R., Oleson, K. W., Otto-Bliesner, B., Phillips, A. S., Sacks, W., Tilmes, S., van Kampenhout, L., Vertenstein, M., Bertini, A., Dennis, J., Deser, C., Fischer, C., Fox-Kemper, B., Kay, J. E., Kinnison, D., Kushner, P. J., Larson, V. E., Long, M. C.,

Mickelson, S., Moore, J. K., Nienhouse, E., Polvani, L., Rasch, P. J., and Strand, W. G.: The Community Earth System Model Version 2
(CESM2), Journal of Advances in Modeling Earth Systems, 12, e2019MS001 916, https://doi.org/10.1029/2019MS001916, 2020.

Doughty, C. E., Keany, J. M., Wiebe, B. C., Rey-Sanchez, C., Carter, K. R., Middleby, K. B., Cheesman, A. W., Goulden, M. L., da Rocha,
H. R., Miller, S. D., Malhi, Y., Fauset, S., Gloor, E., Slot, M., Oliveras Menor, I., Crous, K. Y., Goldsmith, G. R., and Fisher, J. B.: Tropical
forests are approaching critical temperature thresholds, Nature, pp. 1–7, https://doi.org/10.1038/s41586-023-06391-z, 2023.

Döscher, R., Acosta, M., Alessandri, A., Anthoni, P., Arsouze, T., Bergman, T., Bernardello, R., Boussetta, S., Caron, L.-P., Carver, G.,
Castrillo, M., Catalano, F., Cvijanovic, I., Davini, P., Dekker, E., Doblas-Reyes, F. J., Docquier, D., Echevarria, P., Fladrich, U., Fuentes-
Franco, R., Gröger, M., v. Hardenberg, J., Hieronymus, J., Karami, M. P., Keskinen, J.-P., Koenigk, T., Makkonen, R., Massonnet, F.,
Ménégoz, M., Miller, P. A., Moreno-Chamarro, E., Nieradzik, L., van Noije, T., Nolan, P., O'Donnell, D., Ollinaho, P., van den Oord,
G., Ortega, P., Prims, O. T., Ramos, A., Reerink, T., Rousset, C., Ruprich-Robert, Y., Le Sager, P., Schmith, T., Schrödner, R., Serva, F.,
Sicardi, V., Sloth Madsen, M., Smith, B., Tian, T., Tourigny, E., Uotila, P., Vancoppenolle, M., Wang, S., Wårlind, D., Willén, U., Wyser,
K., Yang, S., Yepes-Arbós, X., and Zhang, Q.: The EC-Earth3 Earth system model for the Coupled Model Intercomparison Project 6,
Geoscientific Model Development, 15, 2973–3020, https://doi.org/10.5194/gmd-15-2973-2022, 2022.

Feldpausch, T. R., Phillips, O. L., Brienen, R. J. W., Gloor, E., Lloyd, J., Lopez-Gonzalez, G., Monteagudo-Mendoza, A., Malhi, Y., Alarcón,
A., Álvarez Dávila, E., Alvarez-Loayza, P., Andrade, A., Aragao, L. E. O. C., Arroyo, L., Aymard C., G. A., Baker, T. R., Baraloto, C.,
Barroso, J., Bonal, D., Castro, W., Chama, V., Chave, J., Domingues, T. F., Fauset, S., Groot, N., Honorio Coronado, E., Laurance, S.,
Laurance, W. F., Lewis, S. L., Licona, J. C., Marimon, B. S., Marimon-Junior, B. H., Mendoza Bautista, C., Neill, D. A., Oliveira, E. A.,
Oliveira dos Santos, C., Pallqui Camacho, N. C., Pardo-Molina, G., Prieto, A., Quesada, C. A., Ramírez, F., Ramírez-Angulo, H., Réjou-
Méchain, M., Rudas, A., Saiz, G., Salomão, R. P., Silva-Espejo, J. E., Silveira, M., ter Steege, H., Stropp, J., Terborgh, J., Thomas-Caesar,
R., van der Heijden, G. M. F., Vásquez Martinez, R., Vilanova, E., and Vos, V. A.: Amazon forest response to repeated droughts, Global
Biogeochemical Cycles, 30, 964–982, https://doi.org/10.1002/2015GB005133, 2016.

Forkel, M., Drüke, M., Thurner, M., Dorigo, W., Schaphoff, S., Thonicke, K., von Bloh, W., and Carvalhais, N.: Constrain-
ing modelled global vegetation dynamics and carbon turnover using multiple satellite observations, Scientific Reports, 9, 18 757,
https://doi.org/10.1038/s41598-019-55187-7, 2019.

Gatti, L. V., Basso, L. S., Miller, J. B., Gloor, M., Gatti Domingues, L., Cassol, H. L. G., Tejada, G., Aragão, L. E. O. C., Nobre, C., Peters,
W., Marani, L., Arai, E., Sanches, A. H., Corrêa, S. M., Anderson, L., Von Randow, C., Correia, C. S. C., Crispim, S. P., and Neves, R.
A. L.: Amazonia as a carbon source linked to deforestation and climate change, Nature, 595, 388–393, https://doi.org/10.1038/s41586-
021-03629-6, 2021.

Green, J. K., Konings, A. G., Alemohammad, S. H., Berry, J., Entekhabi, D., Kolassa, J., Lee, J.-E., and Gentine, P.: Regionally strong
feedbacks between the atmosphere and terrestrial biosphere, Nature Geoscience, 10, 410–414, https://doi.org/10.1038/ngeo2957, 2017.

Hajima, T., Watanabe, M., Yamamoto, A., Tatebe, H., Noguchi, M. A., Abe, M., Ohgaito, R., Ito, A., Yamazaki, D., Okajima, H., Ito, A.,
Takata, K., Ogochi, K., Watanabe, S., and Kawamiya, M.: Development of the MIROC-ES2L Earth system model and the evaluation of
biogeochemical processes and feedbacks, Geoscientific Model Development, 13, 2197–2244, https://doi.org/10.5194/gmd-13-2197-2020,
2020.

Hasselmann, K.: Multi-pattern fingerprint method for detection and attribution of climate change, Climate Dynamics, 13, 601–611,
https://doi.org/10.1007/s003820050185, 1997.

Hohenegger, C. and Stevens, B.: The role of the permanent wilting point in controlling the spatial distribution of precipitation, Proceedings
of the National Academy of Sciences, 115, 5692–5697, https://doi.org/10.1073/pnas.1718842115, 2018.

Huntingford, C., Zelazowski, P., Galbraith, D., Mercado, L. M., Sitch, S., Fisher, R., Lomas, M., Walker, A. P., Jones, C. D., Booth, B. B. B., Malhi, Y., Hemming, D., Kay, G., Good, P., Lewis, S. L., Phillips, O. L., Atkin, O. K., Lloyd, J., Gloor, E., Zaragoza-Castells, J., Meir, P., Betts, R., Harris, P. P., Nobre, C., Marengo, J., and Cox, P. M.: Simulated resilience of tropical rainforests to CO2-induced climate change, Nature Geoscience, 6, 268–273, https://doi.org/10.1038/ngeo1741, 2013.

Hurtt, G. C., Chini, L., Sahajpal, R., Frolking, S., Bodirsky, B. L., Calvin, K., Doelman, J. C., Fisk, J., Fujimori, S., Klein Goldewijk, K., Hasegawa, T., Havlik, P., Heinimann, A., Humpenöder, F., Jungclaus, J., Kaplan, J. O., Kennedy, J., Krisztin, T., Lawrence, D., Lawrence, P., Ma, L., Mertz, O., Pongratz, J., Popp, A., Poulter, B., Riahi, K., Shevliakova, E., Stehfest, E., Thornton, P., Tubiello, F. N., van Vuuren, D. P., and Zhang, X.: Harmonization of global land use change and management for the period 850–2100 (LUH2) for CMIP6, Geoscientific Model Development, 13, 5425–5464, https://doi.org/10.5194/gmd-13-5425-2020, 2020.

Kay, J. E., Deser, C., Phillips, A., Mai, A., Hannay, C., Strand, G., Arblaster, J. M., Bates, S. C., Danabasoglu, G., Edwards, J., Holland, M., Kushner, P., Lamarque, J.-F., Lawrence, D., Lindsay, K., Middleton, A., Munoz, E., Neale, R., Oleson, K., Polvani, L., and Vertenstein, M.: The Community Earth System Model (CESM) Large Ensemble Project: A Community Resource for Studying Climate Change in the Presence of Internal Climate Variability, Bulletin of the American Meteorological Society, 96, 1333–1349, https://doi.org/10.1175/BAMS-D-13-00255.1, 2015.

Kendall, M. G.: A New Measure of Rank Correlation, Biometrika, 30, 81–93, https://doi.org/10.1093/biomet/30.1-2.81, 1938.

Kolby Smith, W., Reed, S. C., Cleveland, C. C., Ballantyne, A. P., Anderegg, W. R. L., Wieder, W. R., Liu, Y. Y., and Running, S. W.: Large divergence of satellite and Earth system model estimates of global terrestrial CO2 fertilization, Nature Climate Change, 6, 306–310, https://doi.org/10.1038/nclimate2879, 2016.

Lenton, T. M., Livina, V. N., Dakos, V., van Nes, E. H., and Scheffer, M.: Early warning of climate tipping points from critical slowing down: comparing methods to improve robustness, Philosophical Transactions of the Royal Society A: Mathematical, Physical and Engineering Sciences, 370, 1185–1204, https://doi.org/10.1098/rsta.2011.0304, 2012.

Maher, N., Milinski, S., and Ludwig, R.: Large ensemble climate model simulations: introduction, overview, and future prospects for utilising multiple types of large ensemble, Earth System Dynamics, 12, 401–418, https://doi.org/10.5194/esd-12-401-2021, 2021.

Malhi, Y., Phillips, O. L., Mayle, F. E., Beerling, D. J., Gosling, W. D., and Bush, M. B.: Responses of Amazonian ecosystems to climatic and atmospheric carbon dioxide changes since the last glacial maximum, Philosophical Transactions of the Royal Society of London. Series B: Biological Sciences, 359, 499–514, https://doi.org/10.1098/rstb.2003.1434, 2004.

Maslin, M., Malhi, Y., Phillips, O., and Cowling, S.: New views on an old forest: assessing the longevity, resilience and future of the Amazon rainforest, Transactions of the Institute of British Geographers, 30, 477–499, https://doi.org/10.1111/j.1475-5661.2005.00181.x, 2005.

Mauritsen, T., Bader, J., Becker, T., Behrens, J., Bittner, M., Brokopf, R., Brovkin, V., Claussen, M., Crueger, T., Esch, M., Fast, I., Fiedler, S., Fläschner, D., Gayler, V., Giorgetta, M., Goll, D. S., Haak, H., Hagemann, S., Hedemann, C., Hohenegger, C., Ilyina, T., Jahns, T., Jimenéz-de-la Cuesta, D., Jungclaus, J., Kleinen, T., Kloster, S., Kracher, D., Kinne, S., Kleberg, D., Lasslop, G., Kornblueh, L., Marotzke, J., Matei, D., Meraner, K., Mikolajewicz, U., Modali, K., Möbis, B., Müller, W. A., Nabel, J. E. M. S., Nam, C. C. W., Notz, D., Nyawira, S.-S., Paulsen, H., Peters, K., Pincus, R., Pohlmann, H., Pongratz, J., Popp, M., Raddatz, T. J., Rast, S., Redler, R., Reick, C. H., Rohrschneider, T., Schemann, V., Schmidt, H., Schnur, R., Schulzweida, U., Six, K. D., Stein, L., Stemmler, I., Stevens, B., von Storch, J.-S., Tian, F., Voigt, A., Vrese, P., Wieners, K.-H., Wilkenskjeld, S., Winkler, A., and Roeckner, E.: Developments in the MPI-M Earth System Model version 1.2 (MPI-ESM1.2) and Its Response to Increasing CO2, Journal of Advances in Modeling Earth Systems, 11, 998–1038, https://doi.org/10.1029/2018MS001400, 2019.

Moesinger, L., Dorigo, W., de Jeu, R., van der Schalie, R., Scanlon, T., Teubner, I., and Forkel, M.: The global long-term microwave Vegetation Optical Depth Climate Archive (VODCA), Earth System Science Data, 12, 177–196, https://doi.org/10.5194/essd-12-177-2020, 2020.

Otto, F. E.: Attribution of Extreme Events to Climate Change, Annual Review of Environment and Resources, 48, 813–828, https://doi.org/10.1146/annurev-environ-112621-083538, 2023.

Owe, M., de Jeu, R., and Holmes, T.: Multisensor historical climatology of satellite-derived global land surface moisture, Journal of Geophysical Research: Earth Surface, 113, https://doi.org/10.1029/2007JF000769, 2008.

Parry, I. M., Ritchie, P. D. L., and Cox, P. M.: Evidence of localised Amazon rainforest dieback in CMIP6 models, Earth System Dynamics, 13, 1667–1675, https://doi.org/10.5194/esd-13-1667-2022, 2022.

Richardson, A. D., Keenan, T. F., Migliavacca, M., Ryu, Y., Sonnentag, O., and Toomey, M.: Climate change, phenology, and phenological control of vegetation feedbacks to the climate system, Agricultural and Forest Meteorology, 169, 156–173, https://doi.org/10.1016/j.agrformet.2012.09.012, 2013.

Salati, E., Dall'Olio, A., Matsui, E., and Gat, J. R.: Recycling of water in the Amazon Basin: An isotopic study, Water Resources Research, 15, 1250–1258, https://doi.org/10.1029/WR015i005p01250, 1979.

Scheffer, M., Bascompte, J., Brock, W. A., Brovkin, V., Carpenter, S. R., Dakos, V., Held, H., van Nes, E. H., Rietkerk, M., and Sugihara, G.: Early-warning signals for critical transitions, Nature, 461, 53–59, https://doi.org/10.1038/nature08227, 2009.

Silvério, D. V., Brando, P. M., Macedo, M. N., Beck, P. S. A., Bustamante, M., and Coe, M. T.: Agricultural expansion dominates climate changes in southeastern Amazonia: the overlooked non-GHG forcing, Environmental Research Letters, 10, 104 015, https://doi.org/10.1088/1748-9326/10/10/104015, 2015.

Simmons, C. S., Walker, R., Aldrich, S., Arima, E., Pereira, R., Castro, E. M. R. d., Michelotti, F., Waylen, M., and Antunes, A.: Discipline and Develop: Destruction of the Brazil Nut Forest in the Lower Amazon Basin, Annals of the American Association of Geographers, 109, 242–265, https://doi.org/10.1080/24694452.2018.1489215, 2019.

Song, X., Wang, D.-Y., Li, F., and Zeng, X.-D.: Evaluating the performance of CMIP6 Earth system models in simulating global vegetation structure and distribution, Advances in Climate Change Research, 12, 584–595, https://doi.org/10.1016/j.accre.2021.06.008, 2021.

Swart, N. C., Cole, J. N. S., Kharin, V. V., Lazare, M., Scinocca, J. F., Gillett, N. P., Anstey, J., Arora, V., Christian, J. R., Hanna, S., Jiao, Y., Lee, W. G., Majaess, F., Saenko, O. A., Seiler, C., Seinen, C., Shao, A., Sigmond, M., Solheim, L., von Salzen, K., Yang, D., and Winter, B.: The Canadian Earth System Model version 5 (CanESM5.0.3), Geoscientific Model Development, 12, 4823–4873, https://doi.org/10.5194/gmd-12-4823-2019, 2019.

Tao, S., Chave, J., Frison, P.-L., Le Toan, T., Ciais, P., Fang, J., Wigneron, J.-P., Santoro, M., Yang, H., Li, X., Labrière, N., and Saatchi, S.: Increasing and widespread vulnerability of intact tropical rainforests to repeated droughts, Proceedings of the National Academy of Sciences, 119, e2116626 119, https://doi.org/10.1073/pnas.2116626119, 2022.

Verbesselt, J., Umlauf, N., Hirota, M., Holmgren, M., Van Nes, E. H., Herold, M., Zeileis, A., and Scheffer, M.: Remotely sensed resilience of tropical forests, Nature Climate Change, 6, 1028–1031, https://doi.org/10.1038/nclimate3108, publisher: Nature Publishing Group, 2016.

Volodin, E. and Gritsun, A.: Simulation of observed climate changes in 1850–2014 with climate model INM-CM5, Earth System Dynamics, 9, 1235–1242, https://doi.org/10.5194/esd-9-1235-2018, 2018.

Zhu, Z., Piao, S., Myneni, R. B., Huang, M., Zeng, Z., Canadell, J. G., Ciais, P., Sitch, S., Friedlingstein, P., Arneth, A., Cao, C., Cheng, L., Kato, E., Koven, C., Li, Y., Lian, X., Liu, Y., Liu, R., Mao, J., Pan, Y., Peng, S., Peñuelas, J., Poulter, B., Pugh, T. A. M., Stocker,

B. D., Viovy, N., Wang, X., Wang, Y., Xiao, Z., Yang, H., Zaehle, S., and Zeng, N.: Greening of the Earth and its drivers, Nature Climate Change, 6, 791–795, https://doi.org/10.1038/nclimate3004, 2016.

Ziehn, T., Chamberlain, M. A., Law, R. M., Lenton, A., Bodman, R. W., Dix, M., Stevens, L., Wang, Y.-P., Srbinovsky, J., Ziehn, T., Chamberlain, M. A., Law, R. M., Lenton, A., Bodman, R. W., Dix, M., Stevens, L., Wang, Y.-P., and Srbinovsky, J.: The Australian Earth System
370   Model: ACCESS-ESM1.5, Journal of Southern Hemisphere Earth Systems Science, 70, 193–214, https://doi.org/10.1071/ES19035, 2020.
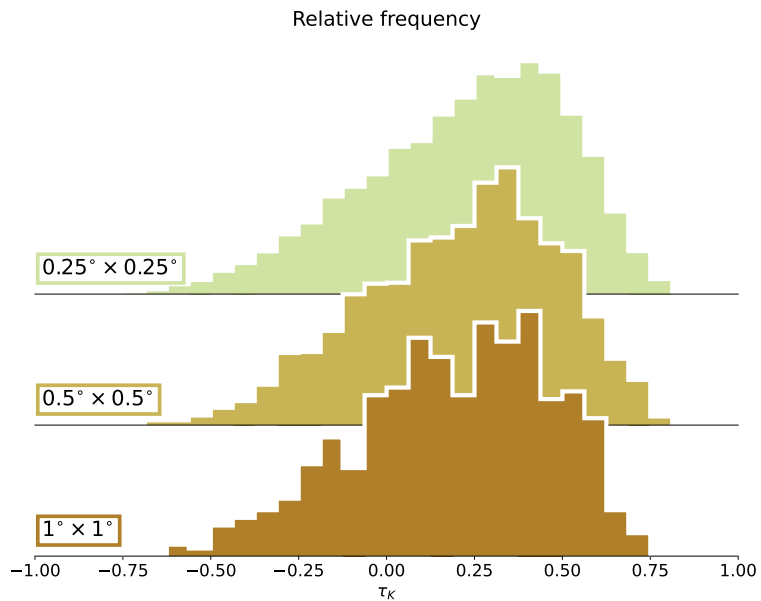
Figure A1. Kendall's τ_K distributions for three different VOD resolutions ($0.25^\circ \times 0.25^\circ$ original VODCA). The means of these histograms are respectively $\bar{\tau}_{K,0.25^\circ} = 0.22$, $\bar{\tau}_{K,0.5^\circ} = 0.22$ and $\bar{\tau}_{K,1^\circ} = 0.21$. We use the $1^\circ \times 1^\circ$ resolution for our analysis since it is the closest to the model resolutions.
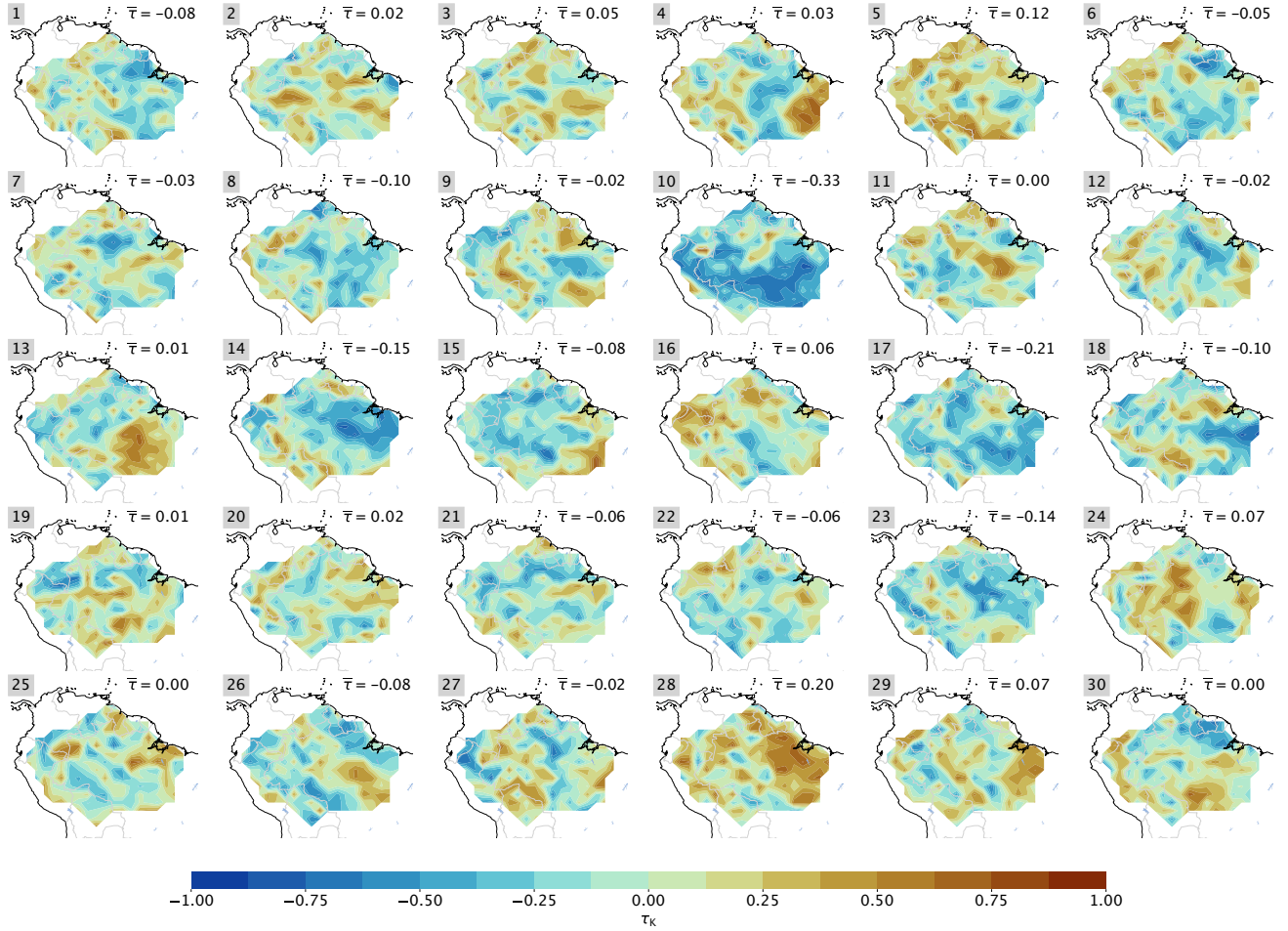
Figure A2. Maps of τ_K of MPI-ESM1-2-LR members according to Fig. 3. The spatial mean for each run is indicated, the observational value is $\overline{\tau}_K = 0.21$ (resolution $1° \times 1°$).
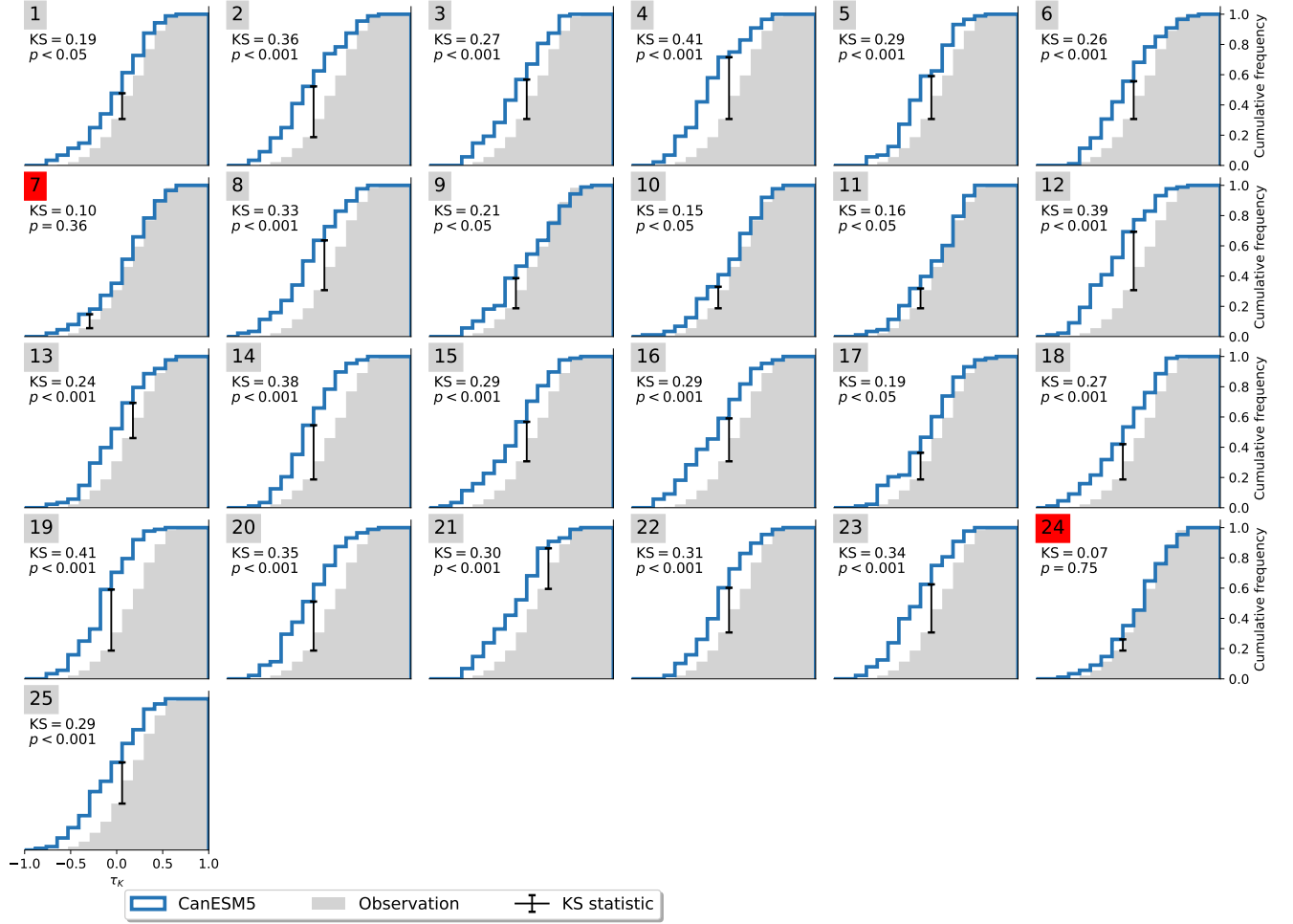
Figure A3. Cumulative distribution functions of τ_K for observations and CanESM5. Significant resemblance ($p > 0.05$) according to KS-test is marked in red.
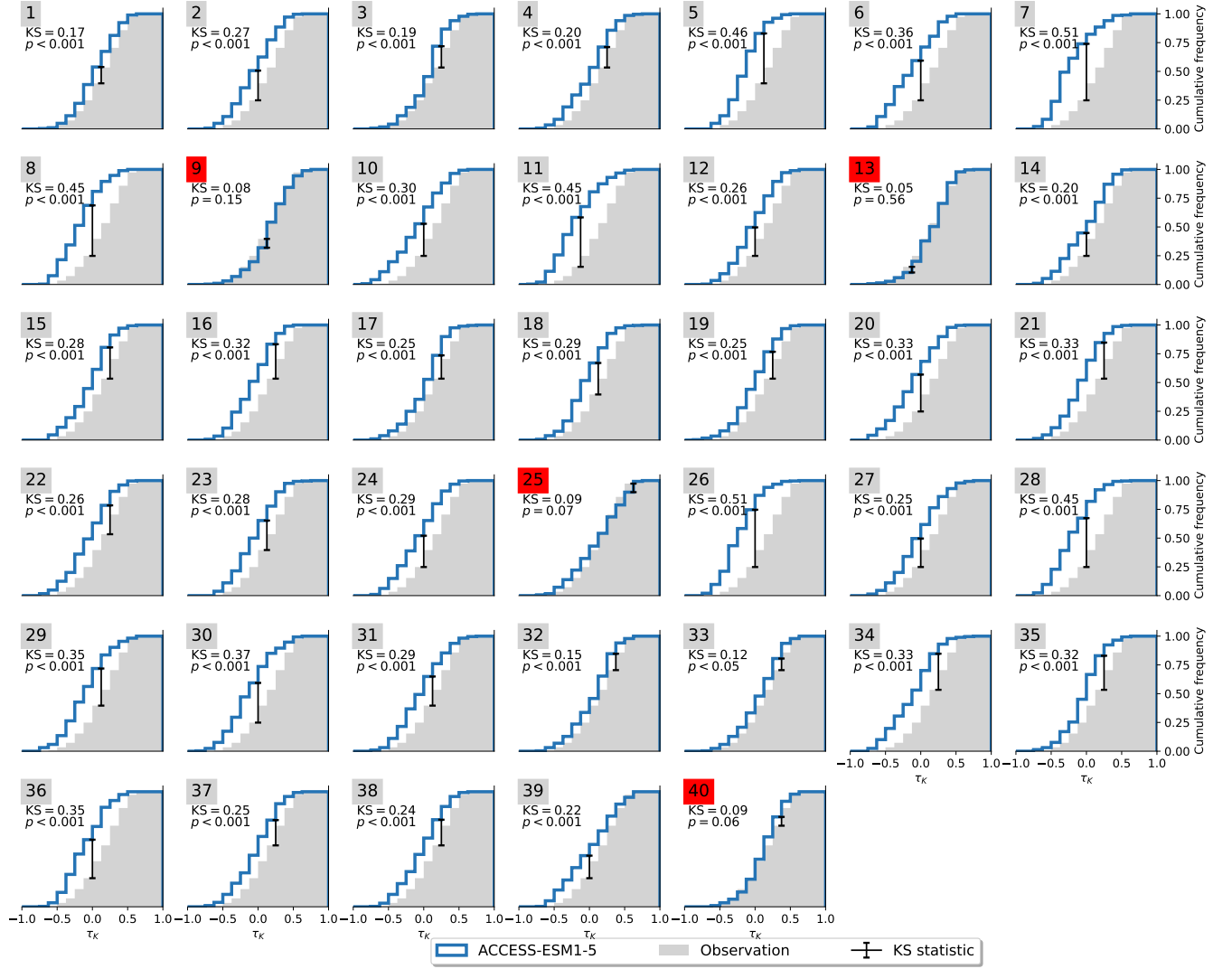
Figure A4. Cumulative distribution functions of τ_K for observations and ACCESS-ESM1-5. Significant resemblance ($p > 0.05$) according to KS-test is marked in red.
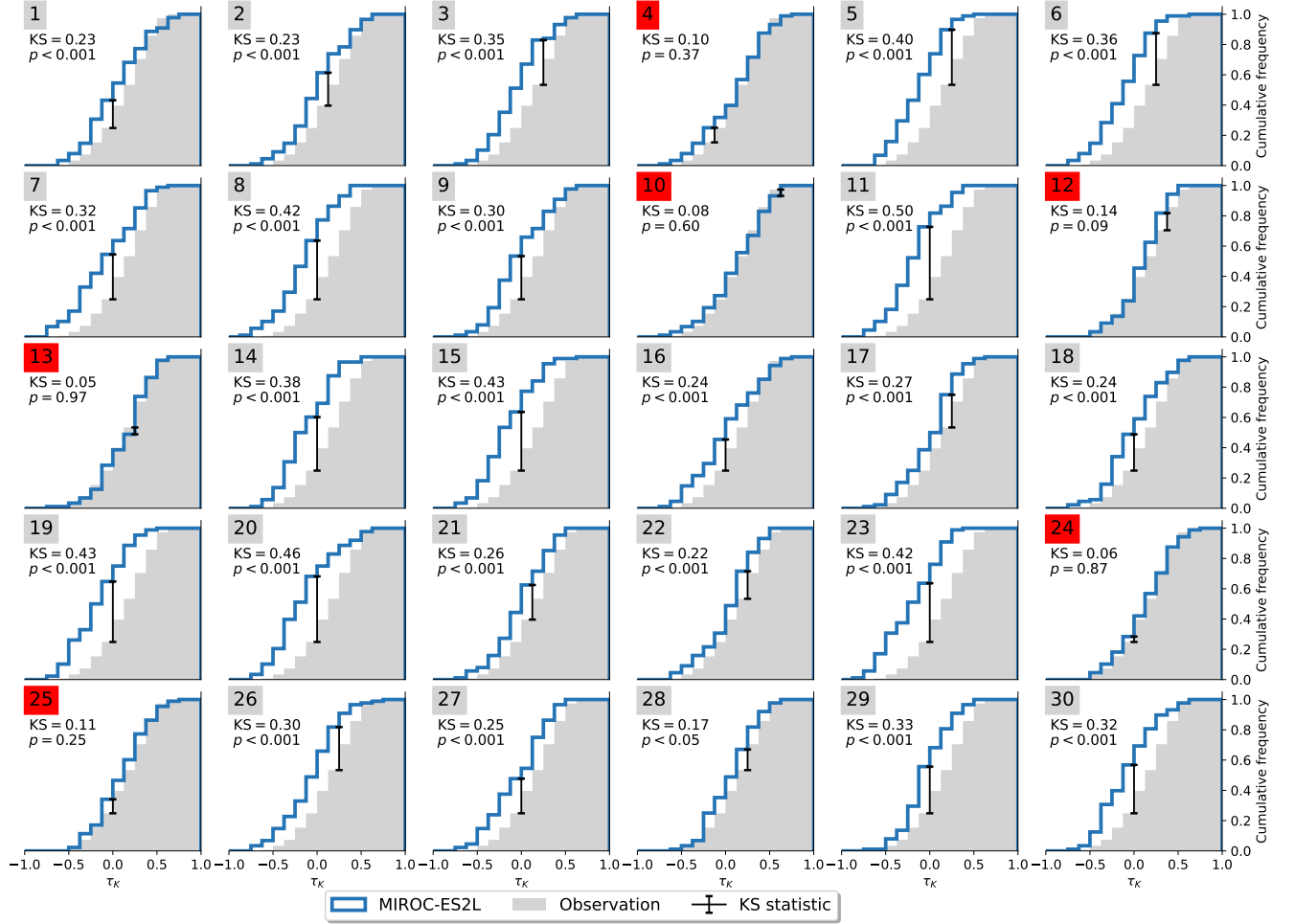
Figure A5. Cumulative distribution functions of τ_K for observations and MIROC-ES2L. Significant resemblance ($p > 0.05$) according to KS-test is marked in red.
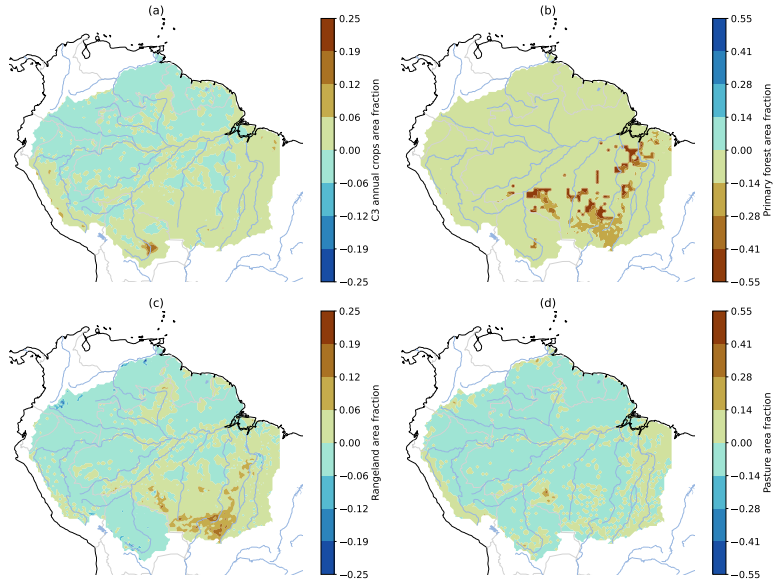
Figure A6. LUCC difference between 2014 and 1990 as prescribed by LUH2 v2h (Hurtt et al., 2020) in CMIP6 models. (a) C3 annual crops (most small-seeded cereal crops), (b) primary forested land, (c) rangeland and (d) pasture. Agricultural activity (a, c and d) increased particularly in the south-eastern regions of the Amazonian, while primary forested land (b) declined in the same areas.
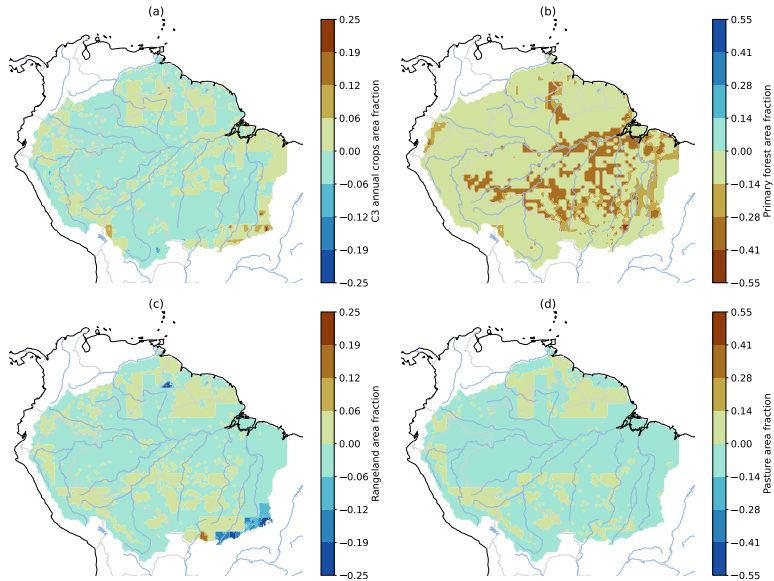
Figure A7. LUCC difference between 2100 and 2015 as prescribed by LUH2 v2f SSP5 (Hurtt et al., 2020) in CMIP6 models. (a) C3 annual crops (most small-seeded cereal crops), (b) primary forested land, (c) rangeland and (d) pasture. Particularly primary forested land reduction (b) effects increasing parts of the Amazon basin.
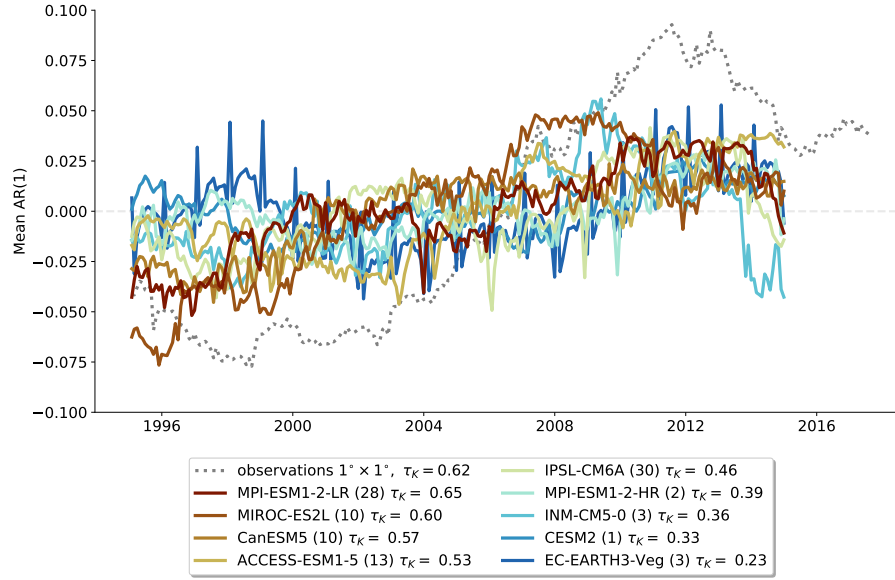
Figure A8. Anomaly of the spatially averaged AR(1) series for observations and best agreeing member for each historical ensemble. The anomaly is computed by subtracting the temporal mean from the time series, and is plotted at the end of the 5 years sliding window. The best agreeing member is shown in parentheses behind the model (the member number shown here agrees with the realization number of the CMIP6 variant ID) and chosen according to its trend statistic τ_K.